Seismic Evaluation of Curved Reinforced Concrete Bridges

K.H. Chao[(1)], Y.C. Sung[(2)], I.C. Tsai[(3)], C.K. Su[(4)], K.W. Chou[(5)], K.X. Wang[(6)], Y.C. Chen[(7)], G.C. Chen[(8)], P.H. Huang[(9)]

[(1)] *Ph.D. student, Department of Civil Engineering, National Taipei University of Technology, Taipei, Taiwan, a825338@gmail.com*
[(2)] *Dean, College of Engineering, National Taipei University of Technology, Taipei, Taiwan, sung.yuchi@gmail.com*
[(3)] *Professor Emeritus, Department of Civil Engineering, National Taiwan University, Taipei, Taiwan, ictsai@ntu.edu.tw*
[(4)] *Associate Researcher, National Center for Research on Earthquake Engineering, Taipei, Taiwan, cksu@ncree.narl.org.tw*
[(5)] *Associate Researcher, National Center for Research on Earthquake Engineering, Taipei, Taiwan, kwchou@ncree.narl.org.tw*
[(6)] *Master, Department of Civil Engineering, National Taipei University of Technology, Taipei, Taiwan, magic2xin@gmail.com*
[(7)] *Ph.D. student, Department of Civil Engineering, National Taipei University of Technology, Taipei, Taiwan, a0989859609@gmail.com*
[(8)] *M.S. student, Department of Civil Engineering, National Taipei University of Technology, Taipei, Taiwan, a26860008@gmail.com*
[(9)] *Associate Vice President, CECI Engineering Consultants, Inc., Taiwan, hsun@ceci.com.tw*

Abstract

This paper devised a procedure of evaluating the seismic performance of a curved bridge of reinforced concrete (RC). Because columns of such a bridge could undertake torques and biaxial moments simultaneously, this procedure requires at least P-M-M interaction curves, which describe for a column section how its axial force and biaxial bending moments interact. This procedure used them to precisely examine if a column fails under biaxial moments. The formation of such curves applied the elastoplastic model of reinforcement and the constitutive laws of confined and unconfined concrete proposed by Mander et al.

Structural analysis software SAP2000 was used to create and analyze the finite element model of a curved bridge existing in Taiwan. The nonlinear behaviors of each column were simulated by both flexural and torsional plastic hinges. Seismic evaluation software SERCBWin helped create and configure biaxial flexural plastic hinges in the SAP2000 structural model. The torsional plastic hinges were configured according to RC torsion theories fed with the properties of column sections, reinforcements, and materials. Investigated was how the seismic response of a curved bridge was affected by varying the peak ground acceleration and acceleration direction of the input earthquake record.

To find the seismic failure orders and patterns of column members, this study created an auxiliary program to examine with respect to P-M-M interaction curves if the maximum biaxial moments of column members exceed the corresponding flexural strengths. On the other hand, whether columns fail under torques was determined by examining how their torsional plastic hinges developed. As the final step of the procedure, the auxiliary program compiled all examination results into an analysis summary of the bridge. We anticipate that such a procedure could help engineers design or perform seismic analysis on curved bridges of reinforced concrete.

Keywords: Seismic Evaluation, Curved Bridge, Reinforced Concrete, Biaxial Bending Moment, Torque.

1. Introduction

The vibration characteristics of a curved bridge often differ from that of a straight bridge. While the top views of a bridge's girders are curved, the support points of all piers are not at a straight line. This geometric characteristic could make the upper and lower structures of a curved bridge undergo bending moments and torques simultaneously. If a curved bridge is subjected to seismic forces, its column members could repeatedly take torques and biaxial bending moments (a straight bridge could avoid the same situation). That means under an earthquake a curved bridge could damage more likely than a straight bridge could. Therefore, it seems worthwhile to study the seismic performance of a curved bridge. Then how to figure out the mechanical characteristics of structural members of a curved bridge becomes necessary. Once grasping those characteristics, engineers could model the nonlinear behaviors of beams and columns (often by configuring plastic hinges) and perform a precise nonlinear analysis that any responsible bridge seismic evaluation requires. In Taiwan, there is still no procedure sufficing to evaluate the seismic performance of a curved bridge.

This study intended to develop a procedure that could precisely evaluate the seismic performance of a curved bridge. In this procedure, it is supposed that structural analysis software SAP2000 is used to model, analyze, and preliminarily evaluate if any bridge member fails in either of its principal axes. And such preliminary evaluation considers no interaction between biaxial bending moments of any pier. While biaxial moment interactions indeed exist, we need to find out the biaxial moment interactions for each pier; and according to the found interaction, the proposed procedure will re-examine if any bridge member fails, which might not fail in the preliminary evaluation. To offer the proposed evaluation procedure the biaxial moment interactions of any bridge member (especially piers), we tried to create the axial force and biaxial bending moment interaction curves, i.e., P-M-M interaction curves. Section 2 briefs how to create such curves. To simulate the seismic nonlinear behavior of a curved bridge by using SAP2000, we focused on precisely configuring plastic hinges of each pier. For curved bridges, in addition to flexural plastic hinges, torsional ones are needed. The auxiliary program SERCBWin can help create the flexural plastic hinges by reading section properties and material details, then configuring them in a SAP2000 model. But for torsional plastic hinges, it requires reliable torsion theories of RC to estimate the hinge properties, and then we may configure them into the SAP2000 model. Section 3 briefs the theories that could help us reasonably simulate the torsional behavior of a RC member. Section 4 represents how the proposed procedure was practiced on an existing curved bridge. Nonlinear dynamic time-history analysis was thoroughly performed for combinations of different PGA values and acceleration directions used to modify the same input earthquake record. The responses of that dynamic history were inspected with respect to the P-M-M interaction curves to find the failure orders and patterns of structural members. What the study found and suggests are concluded in Section 5.

2. Interaction between axial force and biaxial bending moments of reinforced concrete members

Fig. 1(a) shows that a column section takes an axial force P and biaxial bending moments M_x and M_y. The two bending moments are statically equivalent to the same axial force acting eccentrically on the section without bending moments. Such static equivalence requires two eccentricities e_x and e_y with respect to the plastic centroid to locate the axial force as shown in Fig. 1(b). The relationships between the axial force and the bi-axial bending moments may be expressed as $M_x = Pe_x$ and $M_y = Pe_y$.

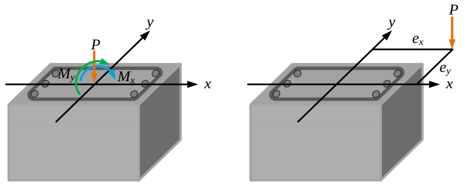

Fig. 1 – Bi-eccentricity loadings

Fig. 2 shows the curves of interactions between P, M_x, and M_y acting on a column section, i.e., P-M-M interaction curves. Two-dimensional interaction curve P-M_x or P-M_y results from a single moment. But P-M_x-M_y interaction curves evolve differently: they result from different biaxial eccentricities under a specified axial force.

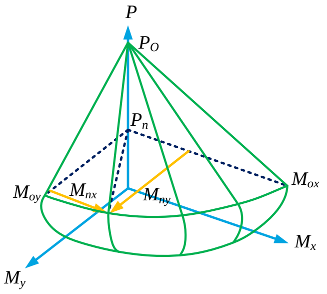

Fig. 2 – P-M-M curves of interactions between the axial force and biaxial bending moments acting on a column section

Fig. 3 shows the procedure of creating biaxial bending moment interaction curves for a column section. Each step of the procedure is illustrated as follows:

1. Prepare the section information including the section dimensions, thickness of the concrete cover, concrete compressive strength, strength of rebars, and θ^*, i.e., the angle between the neutral axis and the principal axis of the section paralleling the direction of the sectional width.

2. Rotate the section by θ^* (See Fig. 3) and then cut the rotated section into fibers of the confined area (See Fig. 4) and that of the unconfined area (See Fig. 5). The shapes of fibers can be irregular polygons. The strain of each fiber ε_i may be determined by the following:

$$\varepsilon_i = \varepsilon_c + \phi \times y^* \ (\varepsilon_c \text{ is negative}) \tag{1}$$

where ε_c is the outermost strain of the compressed area of the section. φ is the curvature. y^* is the distance of a fiber's centroid from the outermost of the compressed area.

3. For fiber i, use its strain ε_i determined by step 2 to compute its stress σ_i according to the constitutive law of confined or unconfined concrete. Then its axial force N_i may be estimated by the following:

$$N_i = \sigma_i \times \Delta A_i \tag{2}$$

where ΔA_i *is* the area of the fiber i. The summation of the axial force for each fiber should be equal to the axial force N acting on the section:

$$\sum_{i=1}^{n} N_i = N \tag{3}$$

If the above equation may be satisfied, we can obtain the biaxial bending moments M_x and M_y acting on the section:

$$M_y = \sum_{i=1}^{n} N_i \times \overline{x_i} \tag{4}$$

$$M_x = \sum_{i=1}^{n} N_i \times \overline{y_i} \tag{5}$$

where $(\overline{x_i}, \overline{y_i})$ is the centroid location of the fiber i in the rotated coordinate system. That location can be obtained from Eq. (6) where (x_i, y_i) is the centroid location in the original coordinate system

$$\begin{pmatrix} \overline{x_i} \\ \overline{y_i} \end{pmatrix} = \begin{pmatrix} \cos\theta^* & \sin\theta^* \\ -\sin\theta^* & \cos\theta^* \end{pmatrix} \begin{pmatrix} x_i \\ y_i \end{pmatrix} \tag{6}$$

4. Under the same axial force N, Keep increasing the curvature φ by $\Delta\varphi$ and then repeating step 2 and 3. So a relationship between biaxial bending moments and the curvature of the section may be created for a fixed axial force. Furthermore, by increasing the axial force and then repeating all the aforementioned steps for the new axial force, we may create a P-M-M relationship for a specified θ^*.
5. By changing θ^* and repeat all the above steps, we can create a complete P-M-M interaction relationship.

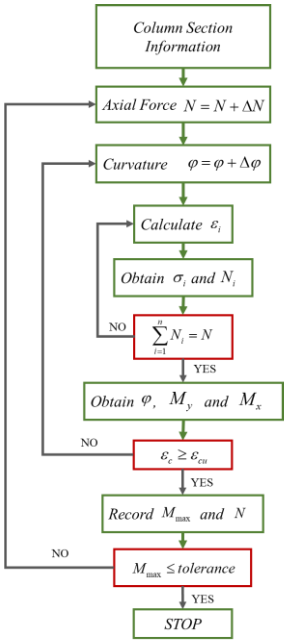

Fig. 3 – Procedure of creating a P-M-M relationship under a specified neutral axis

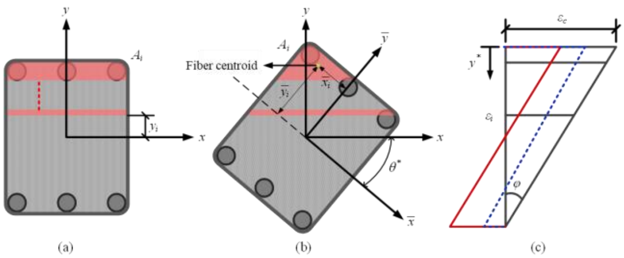

Fig. 4 –Strain measurement of confined fibers under biaxial bending moments

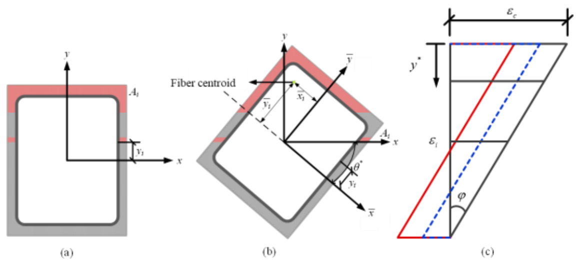

Fig. 5 –Strain measurement of unconfined fibers under biaxial bending moments

3. Torsional modeling of reinforced concrete structural members

Pushover analysis often focuses on figuring out how a structure is affected by axial forces, shear forces, and moments. In fact, many structures could be twisted under earthquakes because they are irregular or loadings over them are not uniformly distributed. To predict precisely the behavior of a structure, we need to study its twisting behavior. Here focused on is how to simulate torsional plastic hinges. Referring to some researches and related specifications of some countries, we chose a de facto way to estimate the torsional stiffness and strength, as what follow.

3.1 Torsional strength

ACI 318-14[1] suggested an estimation of cracking torsional strength, an estimation based on the theory of thin-walled tube and the analogy of space truss. That estimation is derived by equating an actual section with a thin-walled tube whose thickness is $0.75A_{cp}/P_{cp}$ prior to cracking. The area enclosed by the wall centerline is $A_o=2A_{cp}/3$. A_{cp} is the area enclosed by the outside perimeter of the section P_{cp}. For nonprestressed members, the cracking torsional strength T_{cr} may be estimated by using the following:

$$T_{cr} = \frac{1}{3}\sqrt{f_c'}\left(\frac{A_{cp}^2}{p_{cp}}\right) \tag{7}$$

where f_c' is the concrete compressive strength. In addition, the nominal torsional strength T_n may be estimated with what follows:

$$T_n = \frac{2(0.85A_{oh})A_t f_{yt}}{s}\cot\alpha \tag{8}$$

where ACI 318-14 [1] defines A_{oh} as the area enclosed by the centerline of the outmost closed transverse torsional reinforcement. A_t is the area of one leg of a closed stirrup, the area resisting torsion. f_{yt} is the yield strength of transverse reinforcement. s is the spacing of transverse reinforcement. α could be specified with 45°.

3.2 Torsional rigidity

This study estimated torsional rigidity according to the formulae Tavio and Teng [2] suggested. Prior to cracking, a twisted structural member is nearly elastic, and the outmost shear strain of its section could be used to determine its torsional rigidity. According to Saint Venant's principle [3], the torsional rigidity of a uncracked concrete section $(GC)_g$ may be expressed as

$$(GC)_g = G_c\beta_c x^3 y \tag{9}$$

where the shear modulus of concrete $G_c=E_c/2(1+v)$; E_c is the Young's modulus of concrete; v is the Poisson's ratio of concrete; β_c is Saint Venant's torsional constant depending on the ratio of y to x (See Table 1); x is the shorter overall dimension of the rectangular part of the section, y the longer dimension of that rectangular part.

Table 1 – Saint Venant's torsional constant

y/x	1.0	1.2	1.5	2.0	2.5	3.0	4.0	5.0	10	∞
β_c	0.1406	0.166	0.196	0.229	0.249	0.263	0.281	0.291	0.312	0.333

To estimate the post-cracked torsional rigidities of RC members, we used simplified formulae that Tavio and Teng [2] derived from their numerical results. They suggested the following cracking torsional rigidity of concrete $(GC)_{cr}$:

$$(GC)_{cr} = \left(4\mu E_s A_o^2 A_{cp}\right) / \left[p_o^2\left(\frac{1}{\rho_l}+\frac{1}{\rho_h}\right)\right] \tag{10}$$

where μ is a constant. Tavio and Teng [2] believed μ=1.5 best matching the test results. E_s is the elastic modulus of reinforcement (excluding prestressed reinforcement). The length of the enclosed center line of the shear flow p_o=2[(x - t_d/2) + (y - t_d/2)] where t_d is the width of the shear flow. The area enclosed by the center line $A_o = A_{cp} - (2T_a p_{cp} / A_{cp} f_c')$ where T_a is the applied torque. ρ_l is the ratio of the longitudinal reinforcement's area to the gross concrete. ρ_h is the ratio of the transverse reinforcement's area to the gross concrete area.

For RC members reaching their ultimate states, we estimated their torsional rigidities $(GC)_n$ by using the following formula proposed by Tavio and Teng [2]:

$$(\mathrm{GC})_n = \left(4\mathrm{E}_s \mathrm{A}_o^2 \mathrm{A}_{cp}\right) / \left[\mathrm{p}_o^2 \left(\frac{4n\lambda \mathrm{A}_{cp}}{\mathrm{p}_0 \mathrm{t}_\mathrm{d}} + \frac{1}{\rho_l} + \frac{1}{\rho_h}\right)\right] \tag{11}$$

where the estimation of p_o and A_o follows that for Eq. (10). Lampert [4] suggested λ = 3 for the reinforcement to be yielded. But Tavio and Teng [2] Teng believed λ = 4 best matched their test results.

3.3 Configuration on torsional behavior of plastic hinges

We conclude the relationship between the applied torque and twist angle. Fig 6 shows that relationship. Point B and C correspond to the cracking torque T_{cr}. While point A is the origin, the slope of the straight line connecting A with B is the uncracked torsional rigidity $(GC)_g$. The slope of the line connecting A with C is the cracking torsional rigidity $(GC)_{cr}$. The cracking twist angle per length, θ'_{cr}/H, can be computed by what follows:

$$\frac{\theta'_{cr}}{H} = \frac{T_{cr}}{(GC)_{cr}} \tag{12}$$

Where H is the net length of the twisted structural member. Point D represents the ultimate or nomial torsional strength T_n. Because the slope of the line connecting A and D is the ultimate torsional rigidity $(GC)_n$, the ultimate twist angle per length (θ'_n/H) can be computed by what follows:

$$\frac{\theta'_n}{H} = \frac{T_n}{(GC)_n} \tag{13}$$

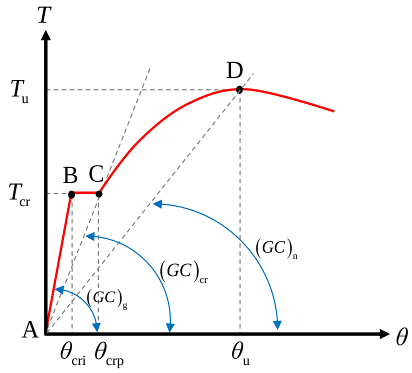

Fig. 6 – Relationship between the applied torque and twist angle

4. Finite element modeling, seismic analysis, and damage inspection of a curved bridge

This study chose the Loop 6 viaduct of Zhonggang System Interchange, the curved bridge to be modeled with finite elements and analyzed. That numerical modeling considered the de facto material strengths, section dimensions, and configuration details of the structural members. While the curved bridge should be treated as an irregular bridge, nonlinear dynamic time history analysis was adopted. To perform that analysis, we estimated the properties of the plastic hinges for each pier and used those properties to define finite elements that suffice to simulate the nonlinear behaviors of piers. The estimation of those properties, therefore, considered the hysteresis loops that describe the nonlinear force-displacement relationships of structural members.

The soil condition of the bridge is classified as the type-1 soil, which would contain medium soil and hard rocks. The superstructure of the bridge comprises prestressed concrete box girders. The bridge has 4 spans that are 27m in spacing. The net width of the bridge is from 8.6 to 11m. The supports are movable along the bridge axis but fixed along all directions perpendicular to the bridge axis. The substructure of the bridge comprises direction foundations and piers. All piers are single reinforced concrete columns. The section of each column is rectangular. Fig. 7 shows the site of the bridge and nearby faults. Fig. 8 shows the plan and elevation views of the bridge.

Fig. 7 – Bridge site and nearby faults

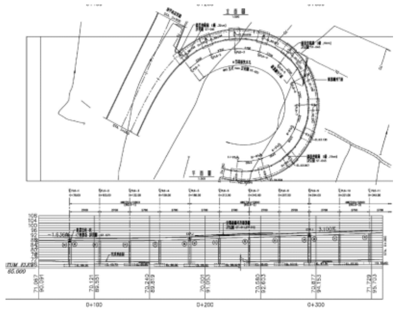

Fig. 8 – Plain and elevation drawings of the bridge

4.1 Structural member information

Table 2 shows the pier configurations of the Loop 6 viaduct of Zhonggang System Interchange, Fig. 9-17 the details of piers. Table 3 shows the material properties of bridge structural members.

Table 2 – Configurations of piers

Pier no.	Foundation type	Girder connection	Rebar arrangement	Pier type	Pier height(m)
PL6-5	Direct	Movable	II	A	19.289
PL6-6	Direct	Rigid	V	D	20.502
PL6-7	Direct	Rigid	V	D	21.039
PL6-8	Direct	Rigid	V	D	21.576
PL6-9	Direct	Movable	II	A	21.639

Table 3 – Properties of bridge structural members

	Box girder	Pier cap	Pier	Foundation
Concrete compressive strength (kgf/cm^2)	420	455	455	280
Rebar tensile strength (kgf/cm^2)	4200 for rebars above 19φ 2800 for rebars below 16φ			
Concrete cover thickness (cm)	-	5	5	-

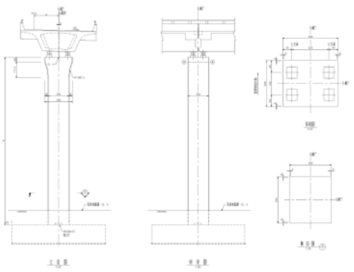

Fig. 9 – Type A pier

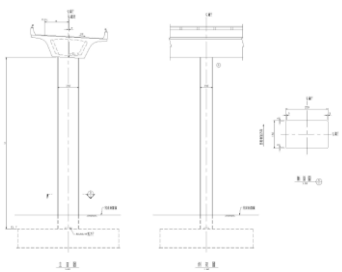

Fig. 10 – Type D pier

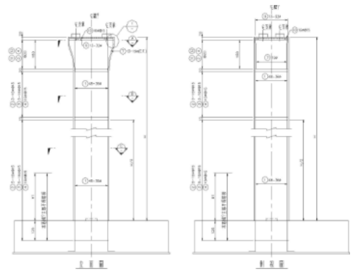

Fig. 11 – Elevation view of pier rebar arrangement type II

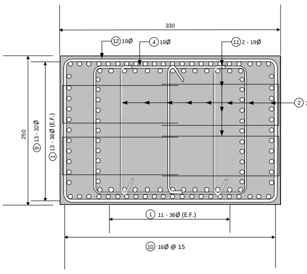

Fig. 12 – Section-A view of pier rebar arrangement type II

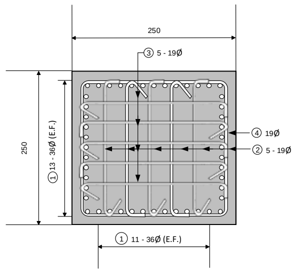

Fig. 13 – Section-B view of pier rebar arrangement type II

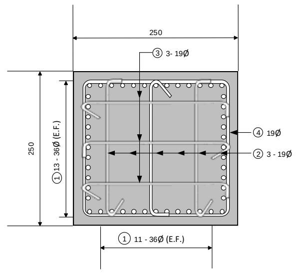

Fig. 14 – Section-C view of pier rebar arrangement type II

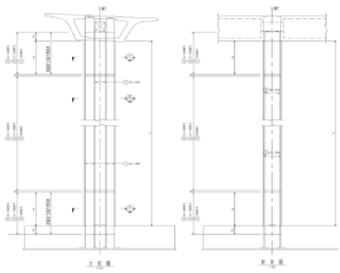

Fig. 15 – Elevation view of pier rebar arrangement type V

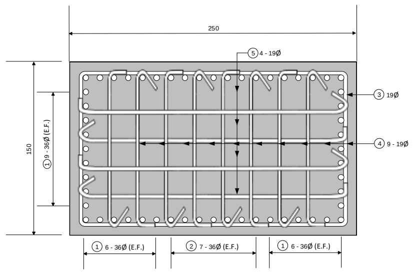

Fig. 16 – Section-A view of pier rebar arrangement type V

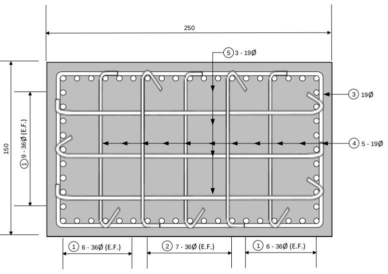

Fig. 17 – Section-B view of pier rebar arrangement type V

4.2 Finite element modeling and modal analysis

According to the configuration of the bridge (See Fig. 18) and its structural member dimensions, SAP2000 was used to create the nodes and elements for the finite element model of the bridge. In that model, all the pier bottoms are connected with equivalent linear springs.

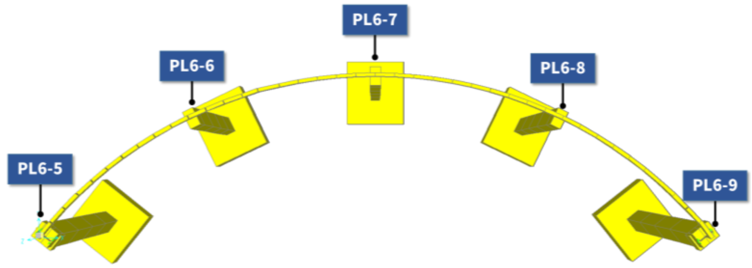

Fig. 18– Plan view of the curved bridge model

Static loadings of the bridge include box girders, the deck, pier caps, and piers. Additional loadings come from the AC pavement, barriers, adjacent span loadings. On two piers PL6-5 and PL6-9, movable supports were simulated with Link elements, capable of moving along their principal axes paralleling the traffic direction. On the SAP2000 model, we performed modal analysis with 100 modes. The summation of the participating mass for each mode exceeds 95% of the total mass of the bridge.

4.3 Configuration and property estimation of plastic hinges

In SAP2000 analysis, the numerical model use beam elements and link elements. The link elements are employed to simulate nonlinear element behaviors. To define a nonlinear link element in a SAP2000 model, the user needs to estimate its nonlinear behavior as the properties of the element. For such estimation, we used SERCBWin to create the properties of plastic hinges and to configure those hinges in a SAP2000 model.

Because curved bridges appear without principal axes, it should consider biaxial moments (M2, M3) for structural members to estimate their plastic hinge properties. So for each pier, we performed such estimation with respect to its local, principal axes. The tops and bottoms of piers are considered where the flexural plastic hinges could take places, while the middle parts of piers were considered capable of developing torsional plastic hinges (See Fig. 19). Plastic hinge properties were estimated for positive and negative directions respectively. The properties of torsional plastic hinges were estimated according to what were mentioned in Section 3. Then all the estimated hinge properties were used to define the link elements in the SAP2000 model.

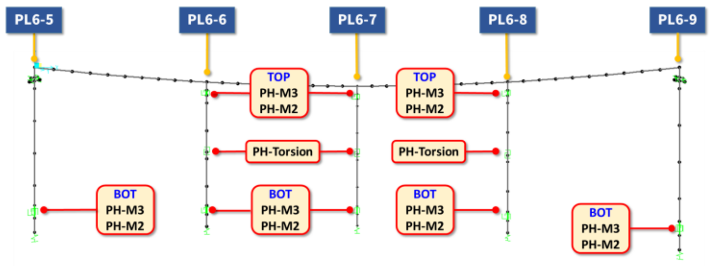

Fig. 19 – Locations to configure plastic hinges

4.4 Seismic analysis and response inspection

To analyze the curved bridge, this study employed a time history of Chi-Chi earthquake. The acceleration time history was recorded by the TAP033 seismic station and represented ground motion along the east-west direction. The acceleration history was transformed to an artificial seismic acceleration history conforming to the corresponding site's design response spectrum of 475-year return period (See Fig. 20). The artificial seismic history (See Fig. 21) was input to the SAP2000 structural analysis in the study.

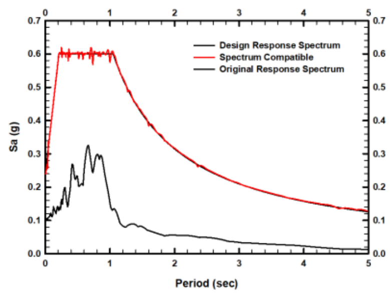

Fig. 20– Design response spectrum of 475-year return period

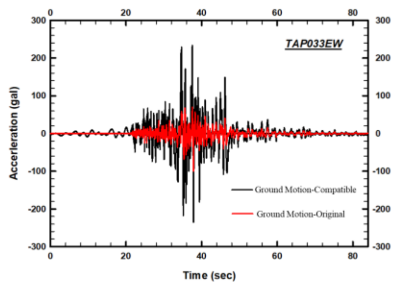

Fig. 21 – Acceleration time history recorded by the seismic station TAP033 (Original) and the artificial acceleration compatible to the response spectrum of 475-year return period

The peak ground acceleration (PGA) of the artificial seismic history was modified as 60, 120, 180, 240, 300, 360, 420, 480, 540, 600, 660, and 720gal for seismic structural analysis. Load cases of SAP2000 were used to specify different angles of acceleration direction, including 0°, 15°, 30°, 45°, 60°, 75°, and 90° (See Fig. 22). Direct-integration time-history analysis was chosen to solve the nonlinear dynamic responses of the curved bridge.

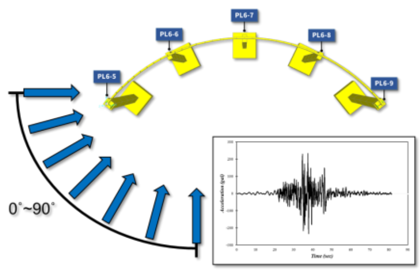

Fig. 22 – Seismic acceleration direction angles specified in SAP2000

If under each combination of the PGA value and acceleration direction angle, no plastic hinges fail, those responses were further inspected with respect to the 3D P-M-M interaction surface. Here we demonstrate such two inspecting stages where the acceleration direction angle is specified with 45°. As shown in Fig. 23-26, the plastic hinges of pier PL6-6 exemplify the nonlinear elements to be inspected. Besides, Fig. 27 shows how developed the torsional plastic hinge of pier PL6-6 for the seismic acceleration direction angle of 45°.

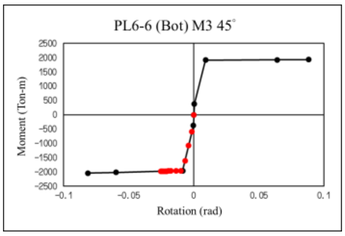

Fig. 23 – Development of the M3 plastic hinge at the bottom of pier PL6-6

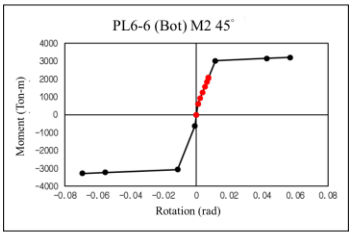

Fig. 24 –Development of the M2 plastic hinge at the bottom of pier PL6-6

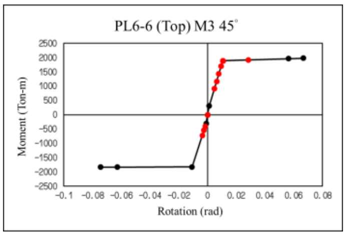

Fig. 25 –Development of the M3 plastic hinge at the top of pier PL6-6

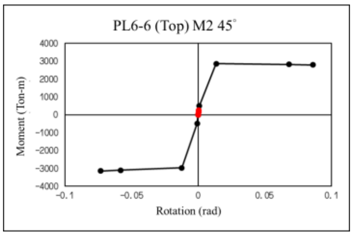

Fig. 26 –Development of the M2 plastic hinge at the top of pier PL6-6

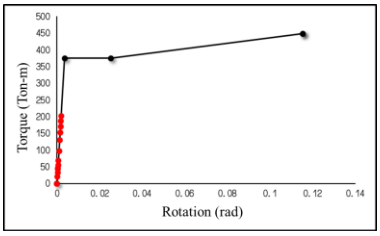

Fig. 27 –Development of the torsional plastic hinge of pier PL6-6

Fig. 28 and 29 show two 3D P-M-M surfaces for response inspection. The two surfaces, drawn with MATLAB, resulted from the seismic acceleration direction angle of 45°. Each point on such a surface represents a different seismic response on the same pier section. Any response point inside a PMM surface is shown in blue. Red is used to show a point outside a PMM surface.

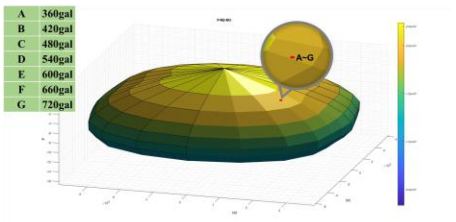

Fig. 28 – P-M-M surface for inspecting the bottom section of pier PL6-6

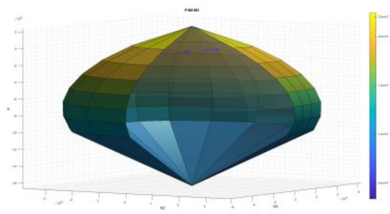

Fig. 29 – P-M-M surface for inspecting the top section of pier PL6-6

4.5 Damage examination using PM ratios

To examine whether a response point is inside or outside a P-M-M surface may be examined by using the PM ratio of the point. Three methods of estimating PM ratios are available: Method 1, 2, and 3 whose formulae are Eq. (13), (14), and (15), respectively. Fig. 30-32 visualize the concepts of those methods, respectively. For a response point, that its PM ratio exceeds 1 indicates the point is outside the P-M-M surface. If that is the case, we recorded the corresponding response, PM ratio, PGA, and acceleration direction angle. Table 4-6 shows the PM ratios estimated by the three methods, respectively. Those ratios were estimated from the seismic responses for the seismic acceleration direction angle of 45°.

$$PM\ ratio = \left(M_{ux} / M_{nx} + M_{uy} / M_{ny} \right) \tag{14}$$

$$PM\ ratio = \left(\overrightarrow{M_{uxy}} / \overrightarrow{M_{nxy}} \right) \tag{15}$$

$$PM\ ratio = \left(\overrightarrow{P_u, M_{uxy}} / \overrightarrow{P_n, M_{nxy}}\right) \tag{16}$$

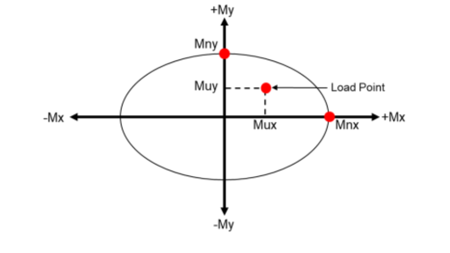

Fig. 30 – Method 1 for PM ratio estimation

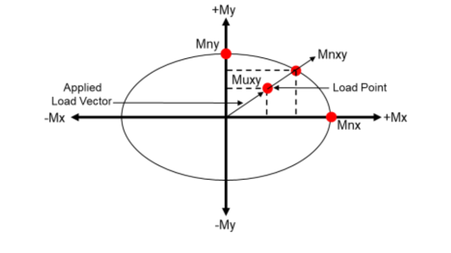

Fig. 31 – Method 2 for PM ratio estimation

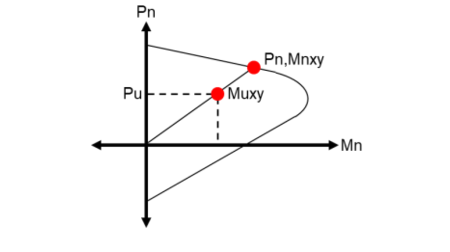

Fig. 32 – Method 3 for PM ratio estimation

Table 4 – PM ratios by Method 1

	PL6-5 (BOT)	PL6-6 (BOT)	PL6-6_ (TOP)	PL6-7 (BOT)	PL6-7 (TOP)	PL6-8 (BOT)	PL6-8 (TOP)	PL6-9 (BOT)
60gal	0.2073	0.4844	0.2358	0.4105	0.1886	0.3568	0.1862	0.2172
120gal	0.2872	0.8303	0.2985	0.6884	0.3334	0.6055	0.2312	0.3868
180gal	0.3387	1.0061	0.3888	0.9772	0.4903	0.8389	0.2807	0.5799
240gal	0.4024	1.0085	0.5337	1.0005	0.6462	1.0036	0.3359	0.7751
300gal	0.5075	1.0147	0.6710	1.0050	0.8053	1.0053	0.3957	0.9706
360gal	0.5933	1.0017	0.8131	1.0144	0.9658	1.0057	0.4478	1.0029
420gal	0.6661	1.0006	0.9572	1.0171	1.0059	1.0021	0.4915	1.0092
480gal	0.7254	1.0060	1.0029	1.0096	1.0029	1.0167	0.5340	1.0141
540gal	0.7888	1.0003	1.0052	1.0003	1.0091	1.0063	0.5762	1.0036
600gal	0.8881	1.0001	1.0037	1.0043	1.0080	1.0182	0.6155	1.0229
660gal	0.9475	1.0056	1.0048	1.0024	1.0027	1.0030	0.6514	1.0188
720gal	1.0075	1.0023	1.0133	1.0018	1.0198	1.0045	0.6878	1.0267

Table 5 – PM ratios by Method 2

	PL6-5 (BOT)	PL6-6 (BOT)	PL6-6_ (TOP)	PL6-7 (BOT)	PL6-7 (TOP)	PL6-8 (BOT)	PL6-8 (TOP)	PL6-9 (BOT)
60gal	0.1366	0.3014	0.2150	0.2761	0.1441	0.2566	0.1375	0.2073
120gal	0.2064	0.5310	0.2890	0.4591	0.2601	0.4343	0.1705	0.3743
180gal	0.2687	0.7776	0.3847	0.6478	0.4009	0.6179	0.2059	0.5568
240gal	0.3424	0.9479	0.4670	0.8221	0.5430	0.7996	0.2479	0.7413
300gal	0.4213	0.9725	0.5977	0.9936	0.6877	0.9795	0.2938	0.9268
360gal	0.4999	1.0010	0.7334	1.0001	0.8350	1.0075	0.3433	1.0008
420gal	0.5795	1.0035	0.8713	1.0066	0.9877	1.0053	0.3933	1.0063
480gal	0.6597	1.0015	0.9679	1.0066	0.9926	1.0093	0.4427	1.0075
540gal	0.7405	1.0015	0.9693	1.0139	0.9950	1.0033	0.4919	1.0078
600gal	0.8210	1.0042	0.9698	1.0061	0.9975	1.0152	0.5374	1.0083
660gal	0.8618	1.0067	0.9704	1.0093	0.9998	1.0021	0.5788	1.0040
720gal	0.9382	1.0055	0.9716	1.0216	1.0000	1.0163	0.6201	1.0089

Table 6 – PM ratios by Method 3

	PL6-5 (BOT)	PL6-6 (BOT)	PL6-6_ (TOP)	PL6-7 (BOT)	PL6-7 (TOP)	PL6-8 (BOT)	PL6-8 (TOP)	PL6-9 (BOT)
60gal	0.0506	0.1967	0.1193	0.1671	0.0724	0.1436	0.0743	0.0790

120gal	0.0943	0.4356	0.1811	0.3569	0.1768	0.3198	0.0951	0.2472
180gal	0.1435	0.7314	0.2790	0.5814	0.3253	0.5318	0.1231	0.4668
240gal	0.2176	0.9369	0.3706	0.7893	0.4853	0.7551	0.1601	0.6888
300gal	0.3090	0.9665	0.5224	0.9925	0.6486	0.9751	0.2075	0.9119
360gal	0.4014	1.0012	0.6821	1.0001	0.8145	1.0091	0.2574	1.0009
420gal	0.4966	1.0043	0.8460	1.0078	0.9862	1.0065	0.3120	1.0076
480gal	0.5926	1.0019	0.9617	1.0078	0.9918	1.0113	0.3686	1.0091
540gal	0.6892	1.0018	0.9633	1.0164	0.9945	1.0041	0.4246	1.0094
600gal	0.7856	1.0052	0.9639	1.0072	0.9973	1.0185	0.4765	1.0101
660gal	0.8346	1.0083	0.9646	1.0110	0.9999	1.0027	0.5238	1.0048
720gal	0.9260	1.0067	0.9659	1.0254	1.0001	1.0198	0.5711	1.0107

5. Conclusion

This study proposed a procedure of evaluating the seismic performance of a curved bridge. Each pier section was considered taking an axial force and biaxial moments. Structural analysis software SAP2000 was employed to create and analyze the model of an existing curved bridge. For precisely simulating the nonlinear behavior of each pier of the curved bridge, flexure and torsional plastic hinges were determined according to RC theories fed with the properties of column sections, reinforcements, and materials. The seismic structural analysis considered different PGA values and acceleration directions to investigate how exhausting variations of seismic input affect the behavior of the curved bridge. Moreover, with respect to the properties of plastic hinges and P-M-M interaction curves, the response solved for each combination of PGA and acceleration direction was inspected to determine the failure order and pattern of each column. What the study found and suggests are briefed as follows:

1. Using SAP2000, we created the numerical model of an existing curved bridge with the de facto material strengths, section dimensions, configuration details, and nonlinear behaviours of structural members. Those nonlinear behaviours were represented by plastic hinges or nonlinear links. The model was precisely created because its period was close to what we expected.

2. Before applying our analysis procedure and methods to an existing curved bridge, we tested them on a single column. Under each combination of the PGA value and acceleration direction angle, the failure orders and patterns of structural members were determined and compiled by examining how developed the moments and torque of each structural member. Such a compilation of structural responses due to various seismic inputs could help grasp the seismic behaviour of a curved bridge.

3. Because in this study, the nonlinear dynamic time-histroy analysis outputed huge result, a program was created to inspect biaxial moments of column sections. This program reads the responses of nonlinear elements exported from users (structural analysis software), chronologically examines if P, M2, M3 are inside the P-M-M surface for each time point, and finally determines which structural members fail.

6. References

[1] American Concrete Institute (2014): Building Code Requirements for Structural Concrete (ACI 318-14) and Commentary (ACI 318R-14).

[2] Tavio T, Teng S (2004): Effective Torsion Rigidity of Reinforced Concrete Members. ACI Structural Journal, 101(2), 252-260.

[3] Saint-Venant (1856): Mémoire sur la torsion des prismes (lu à l'académie le 13 juin 1853). *Mémoires des Savants Etrangers, Mémoires Présentés par Divers Savants à l'Académie des Sciences*, **14**, 233-560.

[4] Lampert P (1973): Postcracking Stiffness of Reinforced Concrete Beams In Torsion and Bending. Analysis of Structural Systems for Torsion, ACI Publication SP-35, American Concrete Institute, 385-433.